Rapid and simultaneous estimation of fault slip and heterogeneous lithospheric viscosity from postseismic deformation

Trever T. Hines and Eric A. Hetland

March 23, 2015

1 Abstract

2 Introduction

Geodetic observations of surface deformation in the months to years following an earthquake are often attributed to afterslip (e.g. *Marone et al.*, 1991), viscoelastic relaxation in the lithosphere (e.g. *Nur and Mavko*, 1974), and/or poroelastic-relaxation (e.g. *Peltzer et al.*, 1998; *Jónsson et al.*, 2003). If postseismic deformation can be entirely described by afterslip, then one could easily constrain the spatial distribution of fault slip with a linear least squares inversion (e.g. *Freed*, 2007; *Bürgmann et al.*, 2002; *Harris and Segall*, 1987), which could then provide insight into the frictional properties of faults (e.g. *Barbot et al.*, 2009). However, postseismic deformation following large (Mw$\geq$7) earthquakes is often attributed to viscoelastic relaxation in the lithosphere (e.g. *Pollitz*, 2003, 2005; *Hetland and Hager*, 2003) or a combination of both afterslip and viscoelastic relaxation (e.g. *Hearn et al.*, 2008; *Rollins et al.*, 2015). In such cases, postseismic deformation can be used to constrain the

lithosphere's viscous properties; however, this is a more difficult task than constraining a slip distribution. Not only are there potentially competing deformation mechanism which must be discerned, finding the viscosity of the lithopshere from postseimsic deformation is a computationally expensive nonlinear inverse problem. Typically, this is approached with a forward modeling grid search method. These forward modeling techniques require the number of unknown parameters being estimated to be small, meaning that significant and potentially inappropriate modeling assumptions must be made (*Hines and Hetland*, 2013; *Riva and Govers*, 2008).

In this paper we propose a relatively fast method to kinematically invert coseismic and postseismic deformation to simultaneously estimate a time dependent distribution of fault slip and an arbitrarily discretized viscosity structure of the lithosphere. Our method is based on an approximation which linearizes the rate of early postseismic deformation with respect to the viscosity of the lithosphere. We demonstrate the efficacy and limitations of our method through a synthetic test.

3 Linearizing early postseismic deformation

On the timescales of postseismic deformation, the lithosphere can be approximated as a Maxwell viscoelastic material where, in the one dimensional form, stress and strain are related by

$$\frac{\partial \varepsilon}{\partial t} = \frac{\sigma}{\eta} + \frac{1}{\mu}\frac{\partial \sigma}{\partial t}. \tag{1}$$

η and μ are viscosity and shear modulus respectively. This constitutive relationship implies that a sudden strain in the lithosphere from an earthquake will instantaneously propagate stresses through the lithosphere elastically (assuming the lithosphere is undergoing quasi-static deformation). Creep will also initiate immediately after the earthquake, where the viscous strain rate in each parcel of the lithosphere will be proportional to the reciprocal of viscostity in that parcel and independent of the viscosity elsewhere. Each parcel will

continue to creep at approximately that rate for as long as the initial elastic stresses from the earthquake are large compared to the stresses transferred through viscous relaxation. In this early postseismic period, creep in each parcel will express itself as surface deformation with an amplitude also proportional to the repicrocal of that parcels viscosity. The surface expression of viscous creep throughout the lithosphere is therefor a linear sum of the surface expression of each parcel. This linearity of early postseismic surface deformation with respect to lithospheric viscosity is demonstrated below using simple anti-plane strain earthquake models where the lithosphere is approximated as a layered halfspace. We use this linearity to construct a simple approximation for early postseismic deformation, which greatly facilitates the inverse problem aimed at estimating the amount of slip on a fault and lithospheric viscosity.

The easiest way to demonstrate how postseismic deformation can be linearized with respect to lithospheric viscosity is with a simple two dimensional earthquake model which consists of a long, vertical, surface rupturing, strike-slip fault oriented in the anti-plane direction and embedded in a viscoelastic horizontal layer overlying a viscoelastic halfspace. We make use of the correspondence principle of viscoelasticity (*Flügge*, 1975), which states that the Laplace transform of deformation in a viscoelastic body has the same form as the Laplace transform of deformation in a elastic body with the same geometry and subjected to the same boundary conditions. The solution for displacement following an earthquake in a viscoelastic lithosphere can then be easily found provided that the solution for displacement in an elastic lithosphere with the same geometry is known. One only needs to replace the shear modulus in the Laplace transform of the elastic solution with the effective viscoelastic shear modulus and then compute the inverse Laplace transform (e.g. *Hetland and Hager*, 2005; *Nur and Mavko*, 1974; *Savage and Prescott*, 1978).

The appropriate elastic solution to start from is given by *Rybicki* (1971). Surface dis-

placements, $u_e(x,t)$, resulting from slip on a fault in a two layered elastic half-space are

$$u_e(x,t) = b(t)\left(\frac{1}{2}W(0) + \sum_{n=1}^{\infty}\Gamma^n W(n)\right) \tag{2}$$

where

$$W(n) = \frac{1}{\pi}\left(\tan^{-1}(\frac{2nH+D}{x}) - \tan^{-1}(\frac{2nH-D}{x})\right) \tag{3}$$

and

$$\Gamma = \frac{\mu_1 - \mu_2}{\mu_1 + \mu_2}. \tag{4}$$

In the above equation $b(t)$ describes cummulative slip on the fault over time and describes both coseismic slip and afterslip. D is the locking depth of the fault, H is the thickness of the upper layer, and μ_1 and μ_2 are the shear modulii in the upper layer and lower half-space respectively.

We then find the Laplace transform of surface displacements in the viscoelastic layered half-space by taking the Laplace transform of eq (2),

$$\hat{u}_e(x,s) = \hat{b}(s)\left(\frac{1}{2}W(0) + \sum_{n=1}^{\infty}\Gamma^n W(n)\right), \tag{5}$$

and replacing μ_1 and μ_2 with the equivalent shear modulii for Maxwell materials in the Laplace domain, $\hat{\mu}_1$ and $\hat{\mu}_2$. The Laplace transform of surface displacements for the viscoelastic model is then

$$\hat{u}_v(x,s) = \hat{b}(s)\left(\frac{1}{2}W(0) + \sum_{n=1}^{\infty}\hat{\Gamma}^n W(n)\right) \tag{6}$$

where

$$\hat{\Gamma} = \frac{\hat{\mu_1} - \hat{\mu_2}}{\hat{\mu_1} + \hat{\mu_2}} \tag{7}$$

$$\hat{\mu_1} = \frac{s}{\frac{s}{\mu_1} + \frac{1}{\eta_1}} \qquad \hat{\mu_2} = \frac{s}{\frac{s}{\mu_2} + \frac{1}{\eta_2}}. \tag{8}$$

To find the surface displacements in the time domain one must find the inverse Lapace transform of eq (6), which is typically done using the method of residues (e.g. *Nur and Mavko*, 1974). However, we are interested in characterizing the behavior of early postseismic deformation and it better serves us to instead perform the inverse Laplace transform with an extension of the initial value theorem. This method is described in the appendix.

For simplicity, we assume that the shear modulus for the viscoelastic lithosphere is homogenous throughout the lithosphere (i.e. $\mu_1 = \mu_2$). We demonstrate in a supplementary ipython notebook that our conclusions here still hold when $\mu_1 \neq \mu_2$. The surface displacements in the time domain are then

$$u_v(x,t) = b(t)\frac{1}{2}W(0) + b(t) * \mathcal{L}^{-1}\left[\sum_{n=1}^{\infty}\hat{\Gamma}^n W(n)\right] \tag{9}$$

Evaluating the above inverse Laplace transform using the method described in the appendix gives us a series expansion of the surface deformation resulting from viscous creep.

$$\begin{aligned} u_v(x,t) =& b(t)\frac{1}{2}W(0) + \\ & b(t) * \left(\frac{\mu}{2\eta_2}W(1) - \frac{\mu}{2\eta_1}W(1)\right) + \\ & b(t) * \left(\left(\frac{\mu^2 t}{4\eta_2^2} - \frac{\mu^2 t}{4\eta_1\eta_2}\right)(W(1) - W(2)) + \left(\frac{\mu^2 t}{4\eta_1\eta_2} - \frac{\mu^2 t}{4\eta_1^2}\right)(W(1) + W(2))\right) + \\ & \ldots \end{aligned} \tag{10}$$

The first term of the series in eq (10) is the surface displacement resulting from the elastic transfer of stresses from slip on the fault. The remaining terms are describing the surface deformation resulting from viscous creep induced by those stresses. Of these remaining terms, the first is the initial rate of surface deformation resulting from viscous creep following a unit of slip and it is convolved with the fault slip history. As suggested, this initial viscous response is a linear expression with respect to the inverse viscosity of the two layers.

If the time since the rupture is sufficiently small compared to the relaxation times of each

layer, η_i/μ, (i.e. the third and following terms in eq. (10) are small), then we can truncate the series and approximate early surface deformation as

$$u_v(x,t) \approx b(t)\frac{1}{2}W(0) + \int_0^t b(t)\left(\frac{\mu}{2\eta_2}W(1) - \frac{\mu}{2\eta_1}W(1)\right)dt. \tag{11}$$

This approximation consists of the elastic response to slip on a dislocation added to the intantaneous viscous response to a unit of slip convolved with the faults slip history. The fact that the instantaneous viscous response is linear with respect to the lithospheric viscosity is a general feature for Maxwell-viscoelastic media and we use a similar approximation when considering an arbitrarily discretized lithosphere in section 3.1. It is therefor valuable to explore the quality of the above approximation for this simple two layered case. Figure 1 shows the series solution from eq. (10) truncated at a sufficiently large N as well as the approximation given by eq. (11). We use shear modulus 32.0 GPa throughout the lithosphere and viscosities 10^{20} and $10^{19}\text{Pa}\cdot\text{s}$ for the top layer and lower half-space respectively. We let b(t) describe 5 meters of instantaneous slip at $t = 0$. It should be noted that a similar approximation was demonstrated by *Segall* (2010) for an elastic layer over a Maxwell viscoelastic half-space. The approximate solution coincides with the series expansion up until about 6 years after the earthquake. At that point, the approximation begins to appreciably overestimate the series solution. In our experience the approximate given by (11) is accurate for about as long as the relaxation time of the weakest layer, which is 10 years in this case.

The approximation given above evidently does not account for the viscous coupling between the two layers since either layers contribution to surface deformation is independent of the other layers viscosity. So one could also consider this approximation as being appropriate for as long as the layers do not significantly transfer stresses between eachother through viscous deformation.

It is worth noting that the instantaneous viscous response of the uppermost layer and lower half-space differ only in sign and in amplitude. In the context of an inverse problem,

this means that it is impossible to use (11) to estimate the absolute viscosity of the two layers, rather it is only be possible to estimate their relative viscosities. This is not a difficult obstacle to overcome because in application we can typically assume that the upper layer has a sufficiently long Maxwell relaxation time such that it is effectively elastic over the postseismic period.

We follow the same procedure from above to find the surface deformation resulting from slip on a strike-slip fault in a three layered viscoelastic halfspace. To do so we start with the solution for a three layer elastic halfspace provided by *Chinnery and Jovanovich* (1972). We evaluate the solution for the viscoelastic problem in our supplementary ipython notebook. Once again, we find that the instantaneous viscous response is linear with respect to the inverse viscosity in each of the three layers and we are able to approximate early postseismic deformation resulting from slip described by $b(t)$ as

$$u_v(x,t) \approx b(t)\frac{1}{2}W(0,0) + \int_0^t b(\theta)\left(\frac{\mu}{2\eta_3}W(1,1) + \frac{\mu}{2\eta_2}(W(0,1) - W(1,1)) - \frac{\mu}{2\eta_1}W(0,1)\right)d\theta \tag{12}$$

where

$$W(n,m) = \frac{1}{\pi}\left(\tan^{-1}(\frac{2nH_2 + 2mH_1 + D}{x}) - \tan^{-1}(\frac{2nH_2 + 2mH_1 - D}{x})\right) \tag{13}$$

and η_1, η_2, and η_3 are the viscosities of the top, middle, and bottom layers respectively, while H_1 and H_2 are the thicknesses of the top and middle layer respectively. We can see that eq. (12) recovers eq. (11) when $\eta_3 = \eta_2$.

At this point, we posit that a similar approximation can be made for an arbitrarily layered lithosphere, at least for the two dimensional case. With this assumption, we can then use eq. (12) to find an instantaneous viscous response kernel and then integrate that kernel over the depth of the lithosphere to find the instantaneous viscous response for an arbitrary depth dependent viscosity structure. If the lithsophere is elastic above the fault depth, D, and

described by $\eta(z)$ below D then early postseismic deformation can be described as:

$$u(x,t) \approx \frac{b(t)}{\pi}\tan^{-1}(\frac{D}{x}) + \int_o^t \int_D^\infty \frac{\mu b(\theta)}{2\pi\eta(\zeta)} \left(\frac{2x}{x^2 + (D+2\zeta)^2} - \frac{2x}{x^2 + (2\zeta - D)^2} \right) d\zeta d\theta. \quad (14)$$

Although the above equation is capable of describing an arbitrary viscosity structure, it falls short of being useful as the forward solution in an inverse problem aimed at estimating lithospheric viscosity. This is because the above equation makes the unphysical assumption that the fault is infinitely long. This would introduce first order errors, which would likely wash out the second order effect of viscosity. Instead, we find eq. (14) useful for making estimates of the depth sensitivity of postseismic deformation.

3.1 Arbitrary Composite Maxwell Model

Motivated by our above results, we make the assertion that the initial rate of surface deformation resulting from an instantaneous dislocation in any two or three dimensional Maxwell viscoelastic medium, which has been arbitrarily discretized into N regions, will have the form

$$\frac{\delta}{\delta t} u(x,t)\big|_{t=0} = \sum_j^N \frac{1}{\eta_j} G_j(x). \quad (15)$$

$G_j(x)$ is the initial rate of surface deformation resulting from creep when the reciprocal of the viscosity in region j is one and zero everywhere else (i.e. elastic). In this sense, $G_j(x)$ can be thought of as a Green's function for the initial rate of surface deformation resulting for viscous creep and we will refer to $G_j(x)$ as the instantaneous viscous Green's function. We verify eq 15 numerically in section 5.5 and save a more rigorous justification for a later paper.

We can then approximate surface deformation as

$$u(x,t) \approx b(t)F(x) + \sum_j^N \int_0^t \frac{b(\theta)}{\eta_j} G_j(x) d\theta \quad (16)$$

where $F(x)$ is the elastic Green's function, which describes the elastic deformation resulting from a dislocation with a unit of slip.

We further generalize this approximation of surface deformation to allow for an arbitrary spatial distribution of slip by using linear superposition. If the elastic defomation in a viscoelastic lithosphere can be described in terms of M elastic dislocation sources, then early surface deformation resulting from both elastic dislocations and viscous creep can be approximated as

$$u(x,t) \approx \sum_{i}^{M} b_i(t) F_i(x) + \sum_{i}^{M} \sum_{j}^{N} \int_0^t \frac{b_i(\theta)}{\eta_j} G_{ij}(x) d\theta. \tag{17}$$

Note that the instantaneous viscous Green's function is dependent upon both the region it represents as well as the dislocation source which induces the viscous relaxation in that region, hence the two indices. If the geometry of the fault and lithosphere are sufficiently simple then $F_i(x)$ and $G_{ij}(x)$ can be determined analytically, as demonstrated in the previous section. For more complicated two or three dimensional geometries, numerical methods are required to compute $F_i(x)$ and $G_{ij}(x)$.

4 Inversion method

The approximation of postseismic deformation given by eq (17) can be cast as an inverse problem aimed at finding the distribution of slip on a fault and an arbitrarily complicated lithosphere viscosity structure from postseismic deformation.

We assume that the slip history in any one direction on each fault patch, $b_i(t)$, can be expressed as P linear terms such that

$$b_i(t) = \sum_{k}^{P} \alpha_{ik} A_k(t). \tag{18}$$

and

$$\int_0^t b_i(\theta)d\theta = \sum_k^P \alpha_{ik} B_k(t). \tag{19}$$

In this paper, $A_k(t)$ consists of either step functions, which describe coseismic slip on a fault patch, and ramp functions, which describe afterslip on a fault patch over a time interval. The approximation given by eq (17) now becomes

$$u(x,t) \approx \sum_i^M \sum_k^P \alpha_{ik} F_i(x) A_k(t) + \sum_i^M \sum_j^N \sum_k^P \frac{\alpha_{ik}}{\eta_j} G_{ij}(x) B_k(t). \tag{20}$$

If we assume that the fault geometry and the elastic properties of the lithosphere are well known then we can numerically compute $F_i(x)$. Likewise, we assume some sufficiently fine discretization of the viscous regions in the lithosphere. This allows us to compute $G_{ij}(x)$ numerically. We are left with the unknown slip parameters, α_{ik}, and unknown viscosities in each region of the lithosphere, η_j.

We estimate these unknown parameters from observations of surface deformation as an inverse problem. Let $\mathbf{u_{obs}}$ be a vector of observed coseismic and postseismic surface displacements at various locations and points in time. Let $\mathbf{m}$ be a vector of all the unknown parameters in α_{ik} and η_j and let $\mathbf{u}(\mathbf{m})$ be a vector of postseismic surface displacements predicted by eq (20). We seek to solve

$$\min \left|\left| \mathbf{f}(\mathbf{m}) \right|\right|_2^2 \tag{21}$$

subject to the constraint that

$$\mathbf{m} \geq 0, \tag{22}$$

where

$$\mathbf{f}(\mathbf{m}) = \begin{vmatrix} \mathbf{W}\left(\mathbf{u}(\mathbf{m}) - \mathbf{u}_{\text{obs}}\right) \\ \lambda \mathbf{L}\mathbf{m} \end{vmatrix}. \tag{23}$$

In the above equation, $\mathbf{W}$ is the inverse of the data covariance matrix. Because this inverse

problem inevitably has nonunique solutions for $\mathbf{m}$, we put additional constraints on the model parameters with the matrix $\mathbf{L}$. In our following synthetic tests we further constrain the solution by minimizing the Laplacian of the spatial distribution of fault slip and lithospheric viscosity. We do so by letting $\mathbf{L}$ be the umbrella operator (*Desbrun et al.*, 1999) such that

$$L_{ij}m_j = \frac{1}{|\mathcal{N}(i)|}\sum_{k\in\mathcal{N}(i)} m_k - m_i \tag{24}$$

where $\mathcal{N}(i)$ denotes the set of all model parameter indices which are spatially adjacent to i.

λ is a penalty parameter, which controls how much we enforce the smoothness constraint. for λ through 10-fold cross validation. We first note that the single regularization parameter, λ, in eq. 21 causes the fault slip parameters, α_{ik}, to be regularized just as much as the viscosity parameters, η_j, which may not be desirable. We instead choose a penalty parameter for the rows in $\mathbf{L}$ regularizing the slip parameters and a seperate penalty parameter for the rows in $\mathbf{L}$ regularizing viscosity. We use 10-fold cross validation to find the optimal pair of slip and viscosity penalty parameters. The optimal pair of penalty parameters are those which minimize the predictive error which is shown in Figure 6.

The slip parameters that we are estimating represent coseismic slip, or afterslip on a fault patch, both of which can typically be assumed to occur in one predominant direction. By imposing the nonnegativity constraint on $\mathbf{m}$, we bound the inferred slip rake on any patch to be between the rake directions of our chosen basis slip directions. Additionally, the nonnegativity constraint on $\mathbf{m}$ prevents unphysical viscosity inferences.

We find the $\mathbf{m}$ that satisfies the above conditions with the Gauss-Newton method (*Aster et al.*, 2013). The best fit model parameters are found by making an initial guess for the solution and then iteratively solving

$$\mathbf{J}(\mathbf{m}^k)\mathbf{m}^{k+1} = -\mathbf{f}(\mathbf{m}^k) + \mathbf{J}(\mathbf{m}^k)\mathbf{m}^k \tag{25}$$

for $\mathbf{m}^{k+1}$. $\mathbf{J}(\mathbf{m}^k)$ is the Jacobian of $\mathbf{f}(\mathbf{m})$ with respect to $\mathbf{m}$ evaluated at $\mathbf{m^k}$. We impose the

nonnegativity constraint on $\mathbf{m}$ by solving eq (25) with a nonnegative least squares algoritm *Lawson and Hanson* (1974).

We find that it is occasionally necessary to constrain the step size for each iteration of eq (25) in order to ensure convergence. We do so in a manner akin to the Levenberg-Marquardt algorithm (*Aster et al.*, 2013). So we instead solve

$$\mathbf{J}^*(\mathbf{m}^k)\mathbf{m}^{k+1} = -\mathbf{f}^*(\mathbf{m}^k) + \mathbf{J}^*(\mathbf{m}^k)\mathbf{m}^k \tag{26}$$

for m^{k+1}, where

$$\mathbf{J}^*(\mathbf{m}) = \begin{vmatrix} \mathbf{J}(\mathbf{m}) \\ \kappa\mathbf{I} \end{vmatrix} \tag{27}$$

and

$$\mathbf{f}^*(\mathbf{m}) = \begin{vmatrix} \mathbf{f}(\mathbf{m}) \\ \mathbf{0} \end{vmatrix} \tag{28}$$

where κ controls the step size for each iteration and varies depending on whether the algorithm is converging.

In a nonlinear least squares algorithm, computing the Jacobian typically is the largest computational burden; however in this case, evaluating the Jacobian of eq (20) requires only a few computationally inexpensive matrix operation. Consequently, our nonlinear least squares algorithm converges to a solution for the unknown parameters α_{ik} and η_j in a matter of seconds on a desktop computer. The main computational burden is in computing $F_i(x)$ and $G_{ij}(x)$ which is done with finite element software and only needs to be done once for a given fault and lithosphere geometry.

Throughout this paper, our initial guess for the model parameters is that there is no slip on any fault patch, and the lithosphere is entirely elastic ($\eta^{-1} = 0$). In our experience, the choice of initial conditions has an insignificant affect on the best fit solution.

5 Synthetic test

5.1 Synthetic postseismic deformation

We demonstrate that our inverse method is capable of recovering fault slip and lithospheric viscosity from postseismic deformation with a synthetic test. We use the finite element software, Pylith (*Aagard et al.*, 2007), to compute the surface deformation resulting from a specified amount of slip on a fault in a lithosphere with a specified viscosity. We then invert this synthetic surface deformation with the method described in the previous section to see if we are able to recover the original model parameters. This synthetic test also serves to demonstrate that eq. (15) as well as eq. (17) are indeed valid for three dimensional earthquake models.

Our synthetic model consists of a 50 km long by 20 km wide strike-slip fault striking north and dipping 60° to the east. The map view of this fault is shown in red in figure 4. Coseismic slip at $t = 0.0$ years is specified to have the distribution shown in figure 2. We also specify afterslip on this fault over the time intervals $t = 0.0$ to $t = 0.5$ and $t = 0.5$ to $t = 1.0$ years. The spatial distribution of slip over these intervals is also shown in figure 2. The moment magnitude of the coseismic slip and cumulative afterslip is 7.2 and 6.7 respectively.

The lithosphere in our synthetic model is Maxwell viscoelastic with homogenous Lamé parameters $\lambda = 32.0$ GPa and $\mu = 32.0$ GPa. The viscosity in the lithosphere decays from $10^{21}\text{Pa} \cdot \text{s}$ ($\tau = 1,000$ years) at the surface to $10^{19}\text{Pa} \cdot \text{s}$ ($\tau = 10$ years) at 75 km depth (figure 3). We will compute displacements at 0.1 year intervals up until 10 years after the earthquake which makes our chosen upper bound on viscosity effectively elastic on these timescales.

We output displacements at 60 randomly chosen locations within a 400 km square centered about the fault. This is intended to roughly correspond with the density of GPS station at a well instrumented plate boundary.

Additionally, we add noise to our displacements which is consistent with what one would

expect from GPS observations. The added noise is temporally correlated with a characteristic timescale of 0.25 years. The temporal covariance is intended to simulate seasonal processes which are typically present in GPS timeseries. The standard deviation of northing and easting displacements is 1.0 mm, and the standard deviation of the vertical displacements is 2.5 mm.

Figure 4 shows the synthetic surface displacement in map view while figure 5 shows a sample displacement time series taken from the location nearest to the fault. The displacements shown in figure 5 are with respect to the locations stationary preseismic position.

5.2 Green's functions

In order to estimate the unknown model parameters from our synthetic surface deformation using the method described in section 4, we must first discretize our fault and lithosphere. We chose to break up the fault segment into 60 4 km by 4 km fault patches. We divided our lithosphere into 10 km thick layers from the surface down to 70 km depth resulting in 8 viscous regions where we will be inferring viscosity. Our discretization will prove to be sufficiently fine to describe the synthetic deformation to within its uncertainty.

The next step is to compute the elastic Green's functions, $F_i(x)$, and instantaneous viscous functions, $G_{ij}(x)$, which will both be done numerically using Pylith. The elastic Greens functions are computed by imposing a one meter slip perturbation on each fault patch and then we use the initial displacements as the elastic Greens functions. We compute Elastic Green's functions for both dip-slip and strike-slip motion.

Each instantaneous viscous Greens function is associated with a source of slip, and subsequent relaxation in a particular viscoelastic region of the lithosphere. This means that we compute $60 \times 2 \times 8 = 420$ viscous Green's functions (the 2 is for each slip direction). These are computed by perturbing an elastic lithosphere with a viscosity of $10^{18}\text{Pa} \cdot \text{s}$ for each of our discretized regions. For each perturbed lithosphere, we impose a meter of slip on each fault patch and the initial rates of surface deformation are used as the instananeous viscous

Green's functions.

We define the basis slip functions contained in $A_k(t)$ as a heaviside function centered at $t = 0.0$ and three ramp functions which increase from 0 to 1 meter of slip over the time intervals $t = 0.0$ to $t = 0.5$, $t = 0.5$ to $t = 1.0$, and $t = 1.0$ to $t = 10.0$. The assumption is that slip on each fault patch can be described in terms of these slip functions. Although our synthetic model does not have any fault slip during the last time interval, we include it to test if postseismic deformation over that interval, which is resulting purely from viscous creep, can be describe with continued fault slip.

5.3 Recovered model

Our best fitting model of slip on the fault is shown in figure 2. The spatial distribution, direction, and magnitude of our inferred coseismic slip is a good match to the synthetic coseismic slip. This is to be expected because the magnitude of coseismic displacments far outweigh their uncertainties (figure 4), giving us an large unobscurred signal to constrain fault slip.

Our inferred afterslip over the first and second half of the year following the earthquake are not as well resolved. This is not surprising because the imposed afterslip over this invertal is an order of magnitude smaller than the coseismic slip, resulting in a smaller signal to noise ratio. Figure 4 shows that displacements over this time period, which are mostly due to afterslip, are appreciably larger than the data noise for only a few near field sites. Although this results in inferrences of afterslip that are not well resolved spatially, the magnitude of inferred slip over this interval is consistent with the synthetic slip. This means that most of the deformation during this time period is being properly attributed to afterslip rather than viscous relaxation.

The inferred slip over the last time interval, 1.0 to 10.0 years following the earthquake, is also consistent with the synthetic model. The seismic moment of slip over this interval is 10^{18}N/m, which is 63 times smaller than that of the coseismic slip. This means that inferred

slip is accounting for, at most, a few mm's of displacement from $t = 1.0$ to $t = 10.0$. This is on order of the data uncertainty meaning that the inferred slip is negligably small. This is encouraging because the surface displacements during this final time interval, which are qualitatively more diffuse, are approriately not being attributed to fault slip. Rather, the displacment during this time interval is inferred to be resulting from viscous relaxation.

The inferred viscosities in each of the eight layers are shown in figure 3a. The recovered viscosities correspond very well with the synthetic model except perhaps for the top layer from 0 to 10 km depth. We used bootstrapping to estimate the uncertainties of the recovered viscosities and we found that the strongest layers near the surface have the highest uncertanties. This may seem counterintuitive because one would expect the shallowest regions of the lithosphere to have the strongest influence on surface displacements and thus be well resolved. However, viscosities greater than $10^{20}\text{Pa}\cdot\text{s}$ are effectively elastic on the timescales of this synthetic test, meaning that a wide range of high viscosities for the upper layers would just as adequately be able to describe the synthetic surface displacements. We find it much more informative to instead look at inferred values of $\frac{1}{\eta_j}$ with depth (figure 3b). We can see now that the uncertainties on inferred inverse viscosities behave much more intuitively. The inferred inverse viscosity of the uppermost region has the lowest uncertianty, while the lower half-space has the least well resolved inverse viscosity.

We note that our inferred viscosities are strongly influenced by the regularization. Indeed, many far less smooth viscosity structures would be able to fit the synthetic data just as well as what is shown in figure 3. Additionally, based on figure 6, larger regularization parameters could have been used at only a slight cost to the models predictive power. That is to say, an even smoother viscosity structure than that shown would also be able to adequately describe the synthetic data.

5.4 solution validation

The fact that our recovered fault slip and lithospheric viscosity are in good agreement with the synthetic model suggests that the approximation given by eq. (17) is accurate over the ten years of synthetic data. We will quantify the accuracy of eq. (17), and thereby eq (15), by running a forward model where the imposed fault slip and lithospheric viscosity are those found in our recovered model. We then compare the displacements from the numerically computed forward model with the displacements predicted by eq. (17). We will refer to the numerically computed displacements at time t as $\mathbf{u}_{\text{true}}(t)$ and the displacments at time t predicted by our approximation as $\mathbf{u}(t)$. We define the approximation residuals as $\mathbf{u}(t) - \mathbf{u}_{\text{true}}(t)$.

Figure 7 shows a map view of the approximation residuals at $t = 10.0$ and $t = 20.0$. The approximation residuals at $t = 10.0$ years are small (mm's) compared to the magnitude of displacements at this time (cm's)(figure 4), indicating that eq. (17) is indeed a fair approximation over these timescales. The validity of eq. (17) is more clearly demonstrated in figure 5, which shows $\mathbf{u}(t)$ (black line) and $\mathbf{u}(t)_{\text{true}}$ (red line) at the site closest to the fault. The numerical solution asymptotically approaches the steady rate of postseismic deformation predicted by eq. (17) as the time goes to zero, as implied by eq. (15). The approximation begins to notably diverge from the numerical solution about 10 years after the earthquake.

The residuals shown in Figure 7 are in the same direction as the viscous deformation (figure 4c) indicating that our approximation consistently overestimates the amount of surface deformation resulting from viscous relaxation. The residuals are larger at the near field sites than at the far field sites with relative magnitude about equal to what is seen in figure 4c. 10 years after the earthquake, the error is consistently on order of the imposed data uncertainty. 20 years after the earthquake, errors become appreciably large for the near field sites.

Figure 7 also shows the root mean square error as a function of time, RMSE(t), which

we define as

$$\mathrm{RMSE}(t) = \frac{||\mathbf{u}(t) - \mathbf{u}_{\mathrm{true}}(t)||_2}{\sqrt{\mathrm{Q}}} \tag{29}$$

where Q is the number of elements in $\mathbf{u}(t)$ and $\mathbf{u}_{\mathrm{true}}(t)$. The root mean square error describes how much we would expect the approximate displacements to deviate from the true displacements for a given time. Generally speaking, our approximation can be considered reasonably accurate when the root mean square error is lower than the observation uncertainty. The RMSE increases quadratically from 0 at $t = 0$ to a few millimeters at $t = 20$. When considering that noise for geodetic observations is also on order of a few millimeters, this approximation appears to be sufficiently accurate for at least up until $t = 10$ years.

6 Discussion

Our method for estimating slip and viscosity from postseismic deformation makes the assumption that the timescale of relaxation in the lithosphere is greater than or about equal to the timescales over which postseismic deformation is observed. Since the lithosphere's relaxation time is generally not well known, there is the added complication of deciding how much of a postseismic timeseries to use in the above described inverse method. We conveniently picked the length of our timeseries to correspond with the weakest relaxation time in the lithosphere; however, the length of the timeseries could have also been determined iteratively. If the approximation given by eq. (17) is incapable of adequately describing obersvations, then it is likely that the timeseries used in the inversion is too long. One can reduce the length of the postseismic timeseries used in the inversion until an adequate fit is found.

Our synthetic data is characterized by transient near field surface deformation followed by a steady rate of more diffuse surface deformation. This is qualitatively similar to postseismic deformation following other large ($\geq$ Mw7) earthquakes ((*Pollitz*, 2003, 2005; *Ryder et al.*, 2007; *Rollins et al.*, 2015)). Some have sought to explain this pattern of surface deformation

using a more complex lithospheric rheology capable of transient deformation. We suggest alternatively that fault creep and a relatively high viscosity lithosphere would also be capable of describing the commonly observed patterns of postseismic deformation. In such case, our method described here would allow us to easily constrain the amount of slip and the lithospheric viscosity necessary to describe observed postseismic deformation

Laboratory studies suggest that the lithospheres rheology is generally nonlinear with respect to stress, contradicting our assumption that the lithosphere is Maxwell viscoelastic. However, the above described approximation assumes that stresses in the lithosphere are not significantly different from the stresses induced from fault slip. Under the assumption of constant stress, a material with a nonlinear rheology will behave as a Maxwell viscoelastic material and it will have an effective Maxwell viscosity. This means that viscosities inferred using the above inverse method can be instead interpretted as the effective Maxwell viscosities for the current state of stress in the lithosphere.

Discuss how the solution found here can be used as a first step in a nonlinear least squares algorithm where the forward problem requires using a FEM rather than eq. 17

7 Conclusion

7.1 Appendix

let $f(t)$ and all of its derivatives be continuous and bounded such that its Laplace transform exists (i.e. of exponential type). We define the Laplace transform of $f(t)$ as

$$\mathcal{L}[f(t)] := \hat{f}(s) := \int_0^\infty f(t)e^{-st}dt. \tag{30}$$

It can be easily shown using integration by parts that the Laplace transform of the n^{th} derivative of $f(t)$ is

$$\mathcal{L}[f^{(n)}(t)] = s^n\hat{f}(s) - \sum_{m=1}^{n} s^{m-1}f^{(n-m)}(0). \tag{31}$$

Since we assert that $f(t)$ and its derivatives are of of exponential type, we know that

$$\lim_{s\to\infty} \mathcal{L}[f^{(n)}(t)] = 0. \tag{32}$$

Substituting eq (31) into eq (32) and then rearranging the terms gives us a recursive formula for $f^{(n)}(0)$ in terms of $\hat{f}(s)$:

$$f^{(n)}(0) = \begin{cases} \lim_{s\to\infty} \left(s\hat{f}(s)\right), & \text{if } n = 0 \\ \lim_{s\to\infty} \left(s^{n+1}\hat{f}(s) - \sum_{m=0}^{n-1} s^{m+1} f^{(n-m-1)}(0)\right), & \text{if } n > 0 \end{cases}$$

We can use eq (33) to construct a Taylor series expansion of $f(t)$ about $t = 0$,

$$f(t) = \sum_{n=0}^{\infty} \frac{f^{(n)}(0)}{n!} t^n. \tag{33}$$

Since $f^{(n)}(0)$ can be expressed entirely in terms of $\hat{f}(s)$, evaluating the above series expansion is effectively the same as performing an inverse Laplace transform on $\hat{f}(s)$.

References

Desbrun, M., Meyer, M., Schrder, P., Barr, A. H. (1999). Implicit fairing of irregular meshes using diffusion and curvature flow. Proceedings of the 26th Annual Conference on Computer Graphics and Interactive Techniques - SIGGRAPH 99, 33, 317324. http://doi.org/10.1145/311535.311576

Ryder, I., Parsons, B., Wright, T. J., Funning, G. J. (2007). Post-seismic motion following the 1997 Manyi (Tibet) earthquake: InSAR observations and modelling. Geophysical Journal International, 169, 10091027. doi:10.1111/j.1365-246X.2006.03312.x

Hetland, E. A., Hager B. H.(2003). Postseismic relaxation across the Central Nevada Seismic Belt. Journal of Geophysical Research, 108(Figure 2), 113. doi:10.1029/2002JB002257

Pollitz, F. F. (2005). Transient rheology of the upper mantle beneath central Alaska inferred from the crustal velocity field following the 2002 Denali earthquake. Journal of Geophysical Research B: Solid Earth, 110, 116. doi:10.1029/2005JB003672

Hetland E a., Hager BH. Postseismic and interseismic displacements near a strike-slip fault: A two-dimensional theory for general linear viscoelastic rheologies. J Geophys Res Solid Earth. 2005;110:1-21. doi:10.1029/2005JB003689.

Bürgmann R, Ergintav S, Segall P, et al. Time-dependent distributed afterslip on and deep below the zmit earthquake rupture. Bull Seismol Soc Am. 2002;92(February):126-137. doi:10.1785/0120000833.

Harris R a., Segall P. Detection of a locked zone at depth on the Parkfield, California, segment of the San Andreas Fault. J Geophys Res. 1987;92:7945. doi:10.1029/JB092iB08p07945.

Jónsson S, Segall P, Pedersen R, Bjornsson G. Letters To Nature. Nature. 2003;424(July):179-183. doi:10.1038/nature01758.1.

Peltzer G, Rosen P, Rogez F, Hudnut K. Poroelastic rebound along the Landers 1992 earthquake surface rupture. J Geophys Res. 1998;103(B12):30131. doi:10.1029/98JB02302.

Pollitz FF. Transient rheology of the uppermost mantle beneath the Mojave Desert, California. Earth Planet Sci Lett. 2003;215:89-104. doi:10.1016/S0012-821X(03)00432-1.

Riva R E M, Govers R. Relating viscosities from postseismic relaxation to a realistic viscosity structure for the lithosphere. Geophys J Int. 2009;176:614-624. doi:10.1111/j.1365-246X.2008.04004.x.

Hines T T and Hetland E A Bias in estimates of lithosphere viscosity from interseismic deformation. Geophys Res Lett. 2013;40(August):4260-4265. doi:10.1002/grl.50839.

Rollins C, Barbot S, Avouac J-P. Postseismic Deformation Following the 2010 M=7.2 : 2 El

Mayor-Cucapah Earthquake : Observations , Kinematic Inversions , and Dynamic Models. Pure Appl Geophys. 2015. doi:10.1007/s00024-014-1005-6.

Marone CJ, Scholz CH, Bilham R. On the mechanics of earthquake afterslip. J Geophys Res. 1991;96(B5):8441-8452.

Barbot S, Fialko Y, Bock Y. Postseismic deformation due to the Mw 6.0 2004 Parkfield earthquake: Stress-driven creep on a fault with spatially variable rate-and-state friction parameters. J Geophys Res Solid Earth. 2009;114:1-26. doi:10.1029/2008JB005748.

Freed AM. Afterslip (and only afterslip) following the 2004 Parkfield, California, earthquake. Geophys Res Lett. 2007;34:1-5. doi:10.1029/2006GL029155.

Segall, Paul. Earthquake and volcano deformation. Princeton University Press, 2010.

Hearn EH, McClusky S, Ergintav S, Reilinger RE. Izmit earthquake postseismic deformation and dynamics of the North Anatolian Fault Zone. J Geophys Res Solid Earth. 2009;114(August 2008):1-21. doi:10.1029/2008JB006026.

Flügge, Wilhelm. Viscoelasticity. Springer-Verlag Berlin Heidelberg, (1975).

Lawson, C. L. and R. J. Hanson (1974), Solving least squares problems, *161*, Englewood Cliffs, NJ: Prentice-hall

Chinnery, M. A. and D. B. Jovanovich (1972), Effect of earth layering on earthquake displacement fields, *Bulletin of Seismological Society of America*, *62*, 1629-1639

Rybicki, K. (19710, The elastic residual field of a very long strike-slip fault in the presence of a discontinuity, *Bull. Seism. Soc. Am.*, *61*, 79-92

Nur, A. and G. Mavko (1974), Postseismic Viscoelastic Rebound, *Science*, *183*, 204-206, DOI: 10.1126/science.183.4121.204

Savage, J. and W. Prescott (1978), Asthenosphere readjustment and the earthquake cycle, *J. Geophys. Res.*, *83*, 3369-3376

Aster, R. C., B. Borchers, C. H. Thurber (2013), Parameter estimation and inverse problems, *Academic Press*

Tikhonov AN, Arsenin VY. Solutions of Ill-Posed Problems. Math Comput. 1978;32:1320-1322. doi:10.2307/2006360.

Aagaard B, Williams C, Knepley M. PyLith: A Finite-Element Code for Modeling Quasi-Static and Dynamic Crustal Deformation. eos. 2007;88(52):T21B - 0592.

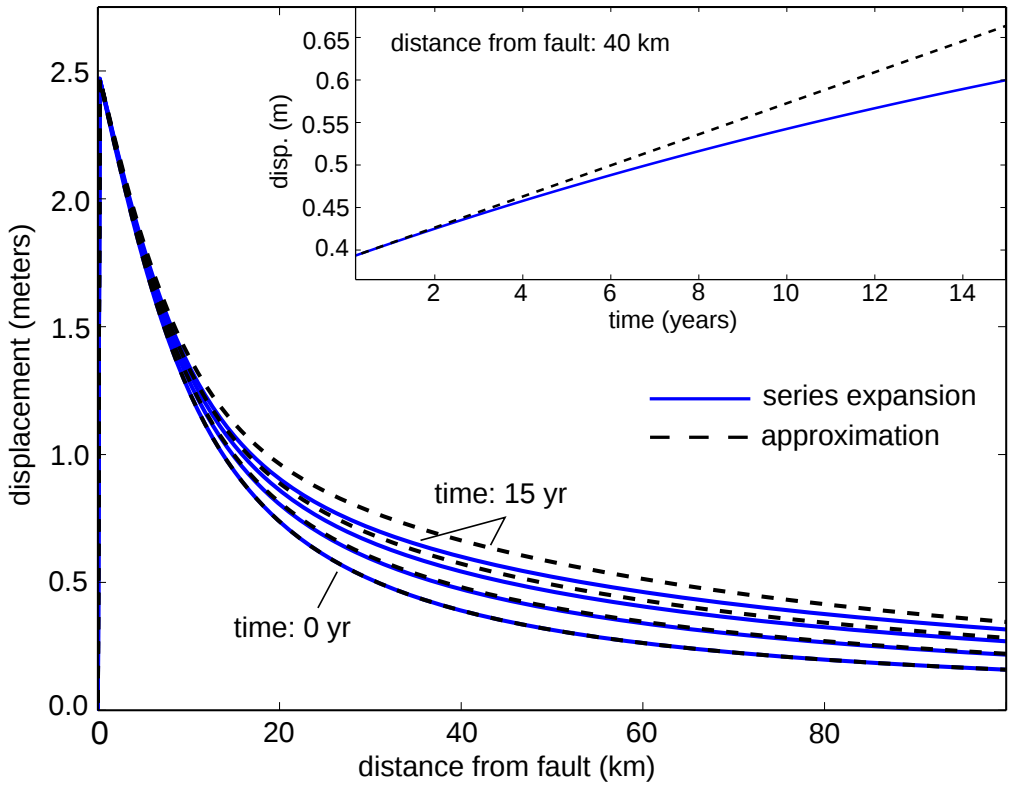

Figure 1: Surface displacements predicted by eq. (10) truncated after five terms (blue) and the approximation given by eq. (11) (dotted black). Displacements are shown at times 0, 5, 10, and 15 years following an earthquake

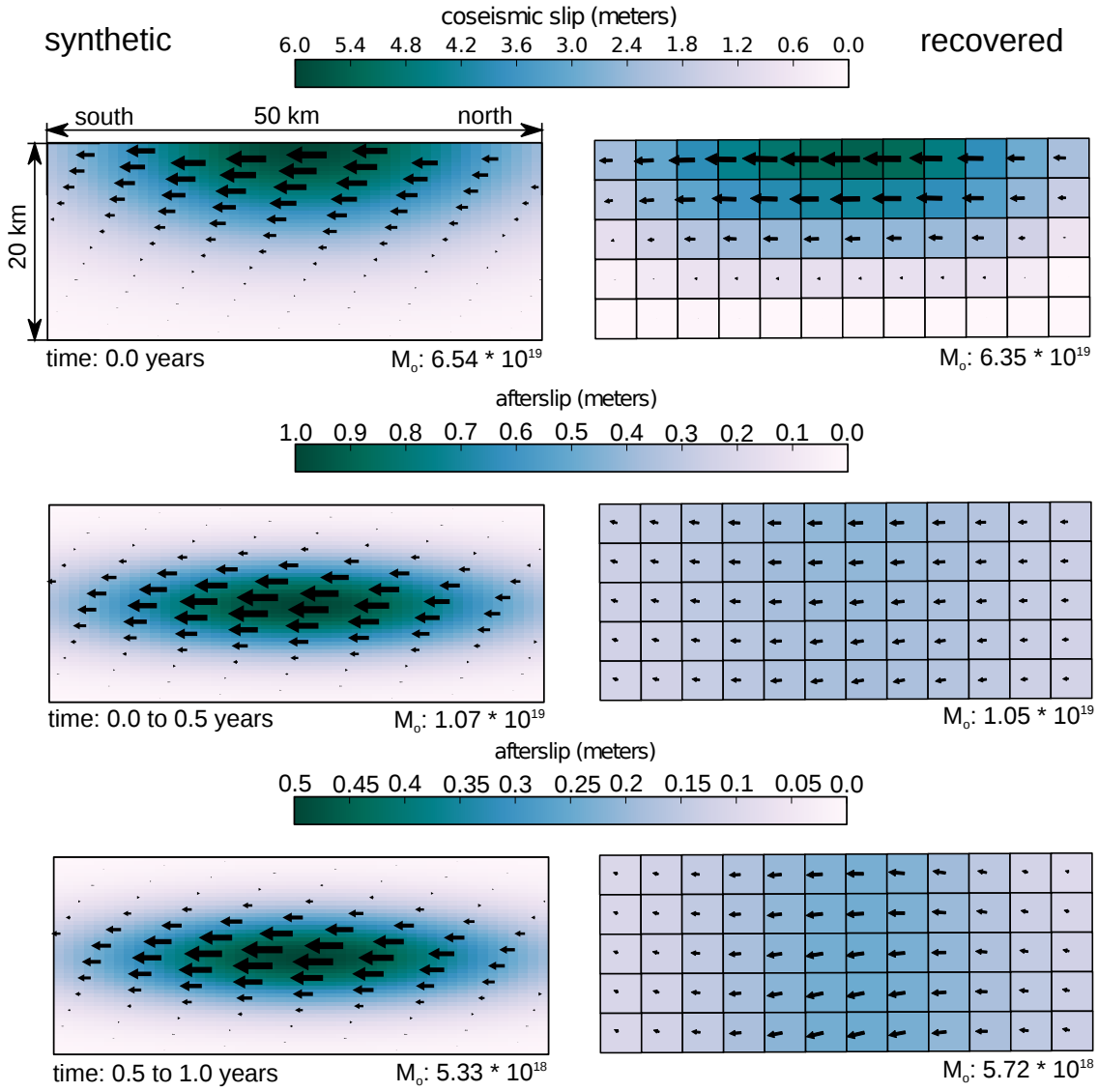

Figure 2: Left: slip distribution imposed in the synthetic model. The panels from top to bottom represent coseismic slip at time = 0.0, and afterslip over the period 0.0 to 0.5 years, 0.5 to 1.0 years, and 1.0 to 10.0 years. Colors indicate magnitude of slip and arrows indicate direction of slip. Right: Slip recovered from inverting the synthetic surface deformation.

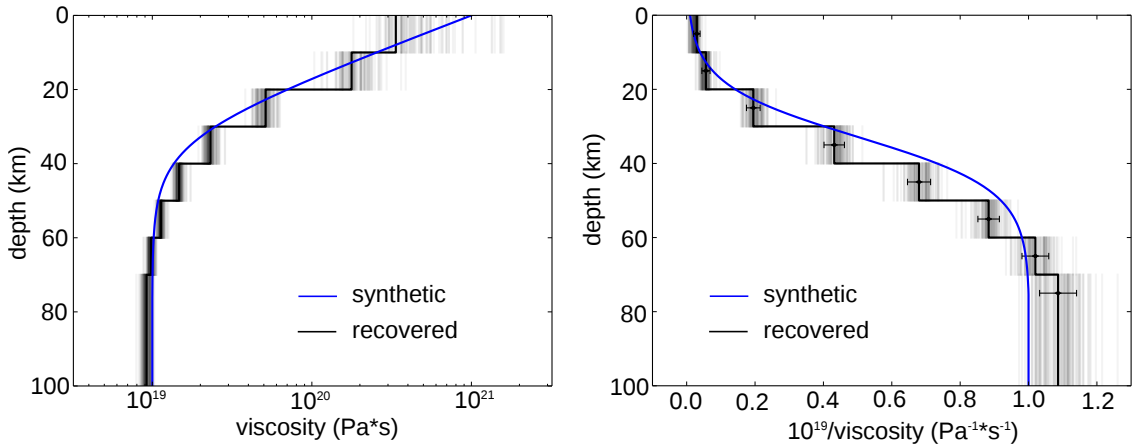

Figure 3: Synthetic and recovered lithospheric viscosity strucutures. Blue line indicates viscosity structure imposed in the synthetic test. Black line indicates viscosity structure inferred from the synthetic surface displacement. Semi-transparent lines are recovered models found through bootstrapping and indicate the degree of uncertainty on the inferred viscosity structure. The left and right panels show the same information under different projections

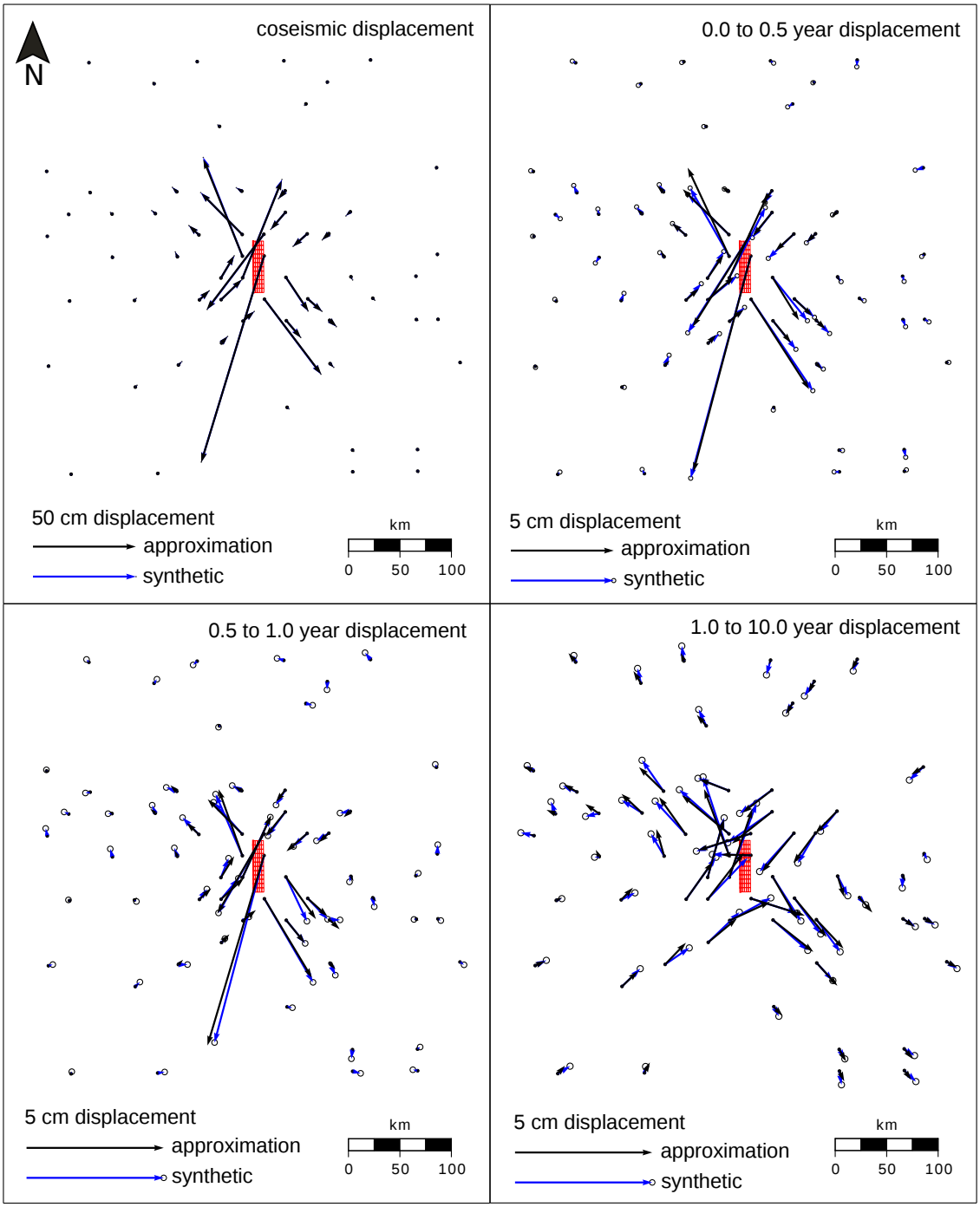

Figure 4: Synthetic surface displacements (blue) and best fitting surface displacements (black). Vertical displacements are used in the inversion but are not shown here. The top left panel shows coseismic displacements and the remaining panals show the displacements over the indicated time intervals. Red dot indicates the position whos time series is shown in figure 5

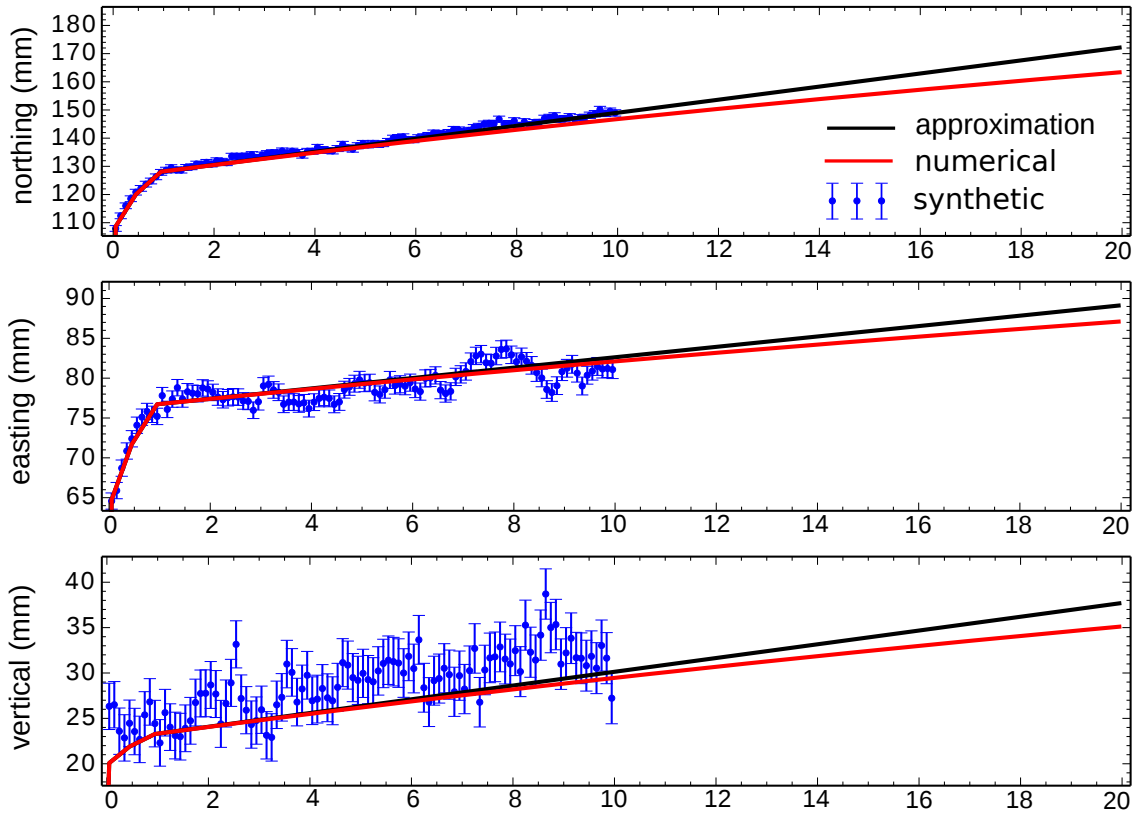

Figure 5: Displacement time series for the position shown in figure 4 (blue) and best fitting surface displacements using the approximation from eq. (17) (black). The red line indicates surface displacements computed using Pylith where the inferred slip distribution and viscosity structure are used as input. The longevity of the approximation is indicated by when the black are red lines diverge

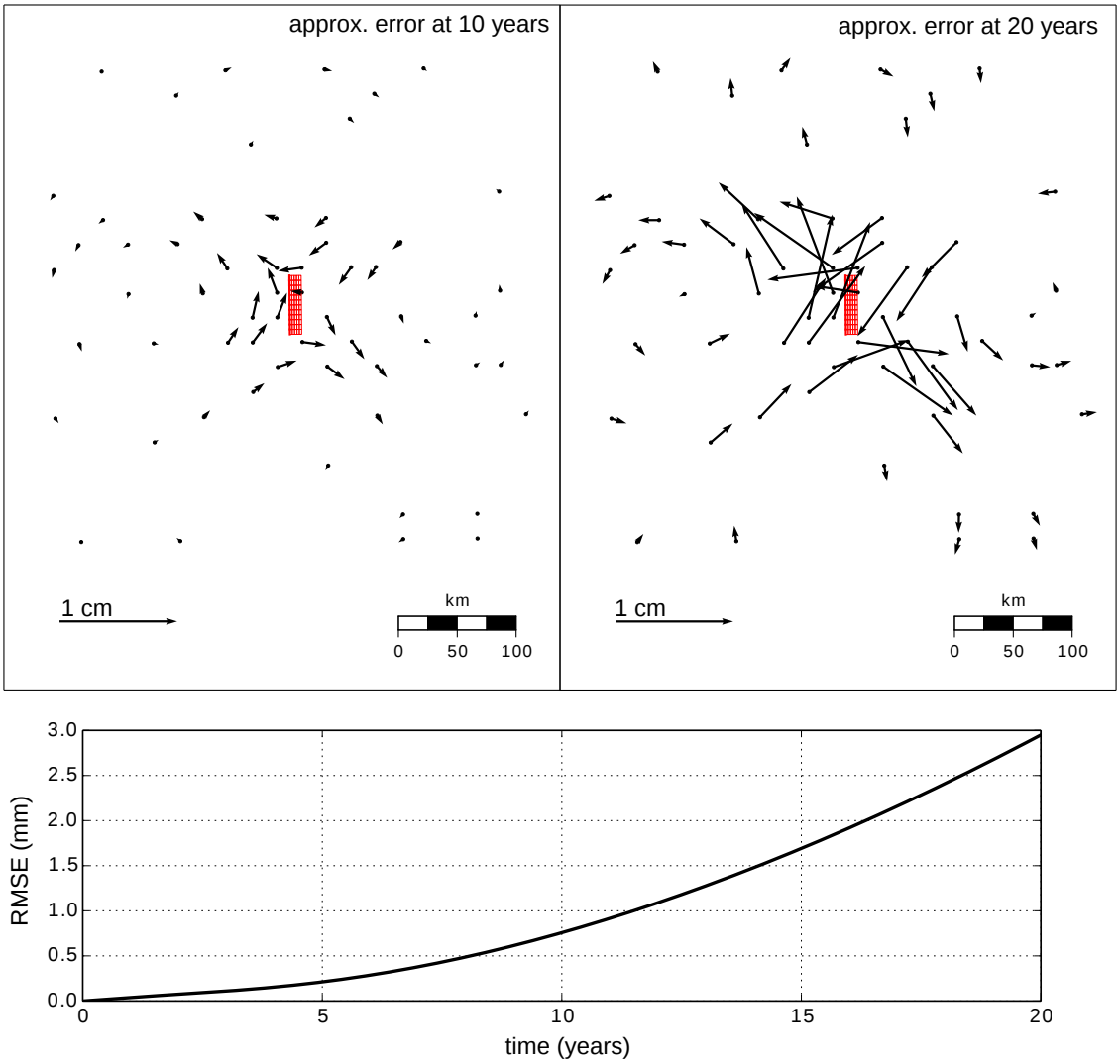

Figure 6: Difference between the surface displacement approximation and the numerically computed surface displacements. Top left panel shows the difference 10 years after the earthquake and the top right panel shows the difference at 20 years. The bottom panel shows the root mean square of the approximation error over time.